Supporting Information for

# Rediscovering the Intrinsic Mechanical Properties of Nanocrystalline Indium Arsenide Bulk

Shuaiqi Li[a], Jiawei Zhang[b], Shixue Guan[a], Ruiang Guo[a], and Duanwei He[*,a,c]

***a*** Institute of Atomic and Molecular Physics, Sichuan University, Chengdu, 610065, China

***b*** Beijing National Laboratory for Condensed Matter Physics and Institute of Physics, Chinese Academy of Sciences, Beijing, 100190, China

***c*** Key Laboratory of High Energy Density Physics and Technology of Ministry of Education, Sichuan University, Chengdu, 610065, China

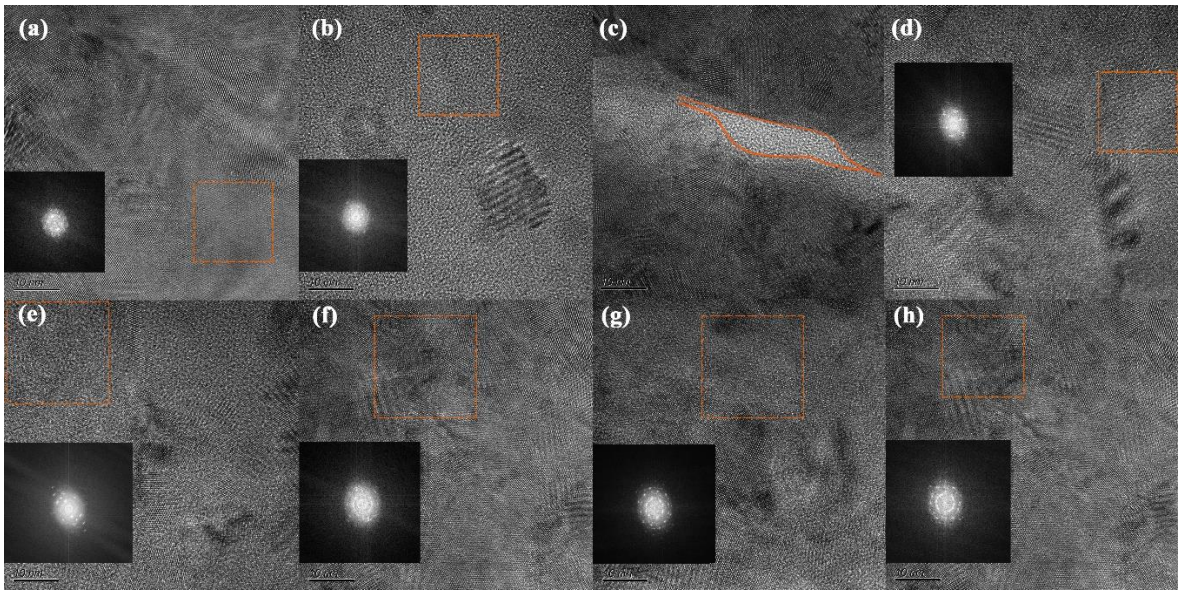


Fig.S1 TEM series atlas with a field of view scale of 10 nm. The illustrations are all FFT transformation modes in the red frames.

The amorphous regions shown in Fig.1e are not widely present in the sample. Fig.S1 shows a TEM atlas with a field size of 10 nm in an R4-InAs sample. The amorphous region shown in Fig.1e is observed only in one of the sheets and is between two crystal clusters. FFT transformation modes in the red frames indicates the polycrystalline features of them. A rough estimate of the proportion of amorphous components in the existing results, through the analysis of Gatan Digital Micrograph, shows that the amorphous region is 236.17 $nm^2$, accounting for 0.4 % of all existing 10 nm FOV images. Although this analysis is sketchy, we believe that the effect of such a small proportion of amorphous region on hardness should be small. The sample after annealing did not observe TEM, but annealing treatment does not lead to an increase in amorphous regions theoretically, as a consequence, the effect of second phase as amorphous on hardness should be controllable.

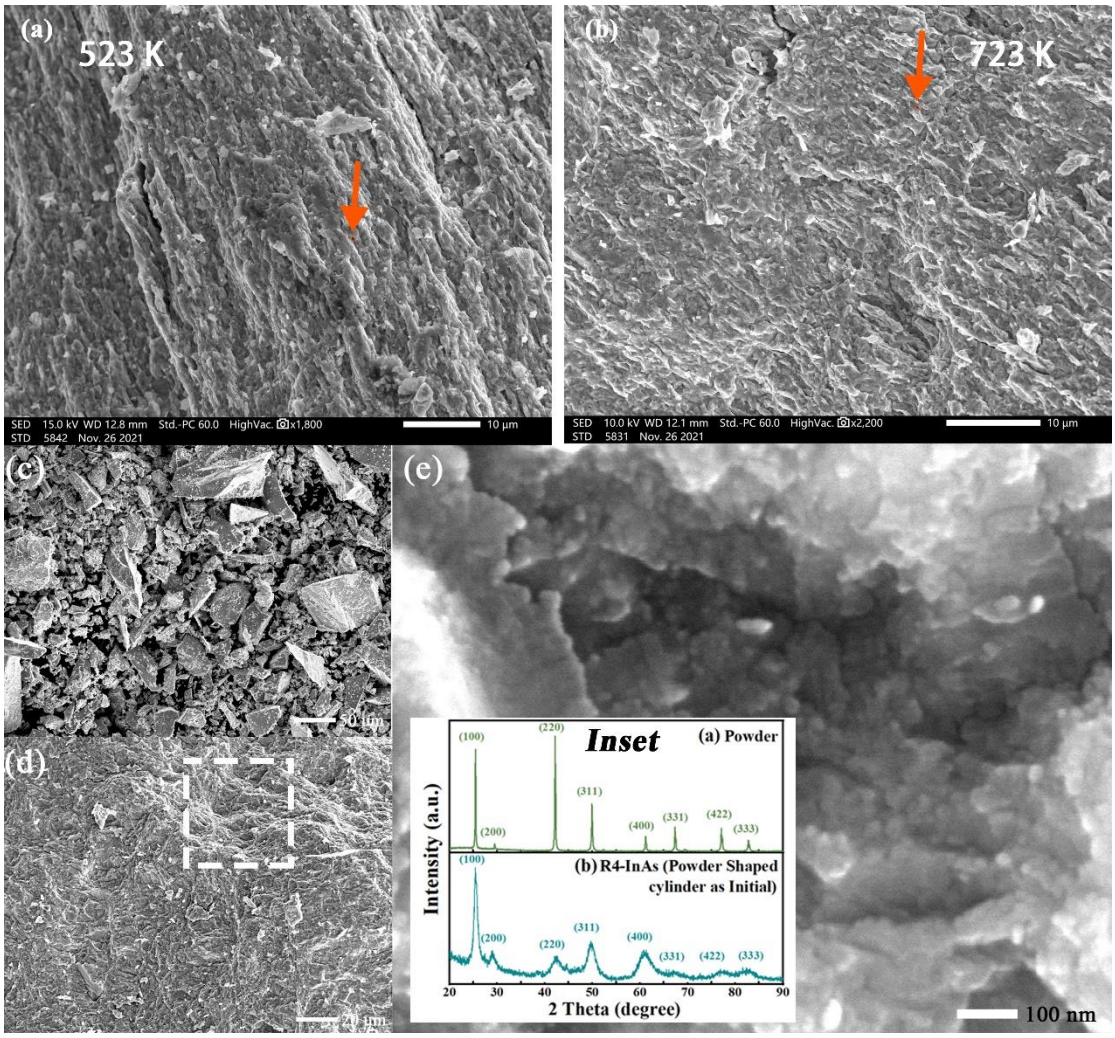


Fig.S2 SEM images of fresh fracture surface for (a) 523 K and (b) 723 K annealed sample. SEM images of power-group experiments (c) initial material, (d-e) fresh fracture surface for powder shaped sample after 4-cycle transition.

The physics state of the sample after annealing, including phase purity, pore distribution, amorphous structure ratio, etc., is critical to its mechanical propertie. In terms of morphology characterization after annealing, Fig.S2(a-b) in support information show SEM images of fresh fracture surface for 523 K and 723 K annealed samples, respectively. Since the phase transition of InAs belongs to diffusion type in terms of atomic migration mode, the interface after phase transition presents an irregular microscopic morphology. The phase transition process is accompanied by the breaking of chemical bonds in the parent phase and the reconstruction of them in new phase, which is why reciprocating pressure-induced phase transition technology can rapidly reduce the grain-size in InAs structure. The red circles in Fig.S2(a-b) indicate the visible pore in SEM image, which appears more regular in annular, but only single-digit pores of about 0.3 um are observed in a large field of view at the 10 um scale.

Based on this, we believe that the pore density of the sample in different annealed states is very small, and the influence on hardness on the macroscopic level can be ignored. In fact, the bonding behavior during the InAs phase transition is so strong that this low porosity phenomenon can also be observed in experiments using InAs powder as a control group. Fig.S2(c) is the polycrystalline InAs powder used with the size of particles distributed in 1~100 um. After using the same experimental conditions as the single-crystal bulk, the fracture surface shows a similar structure to that one as single-crystal bulk initializer, and no significant presence of pore can be observed.

Unfortunately, we tried to test the direct density of the sample using the drainage method and the exhaust method, and since the density of InAs is high but the mass that recovered from high-pressure cell is insufficient, the density values that can be obtained are in obviously unreliable interval (already greater than the theoretical density and cannot be measured repeatably). Consequently, we consider the annealed sample to be dense by the combination of the scanned SEM structures with the characteristics of less pores. Fig.S2(e) is a magnification of the white dotted area in Fig.S2(d), which can observe individual grains on the order of 10 nm. The XRD patterns of initial material and sample after 4 cycles shown in the insertion image also shows the significant nano-broadening while phases are pure InAs-I.

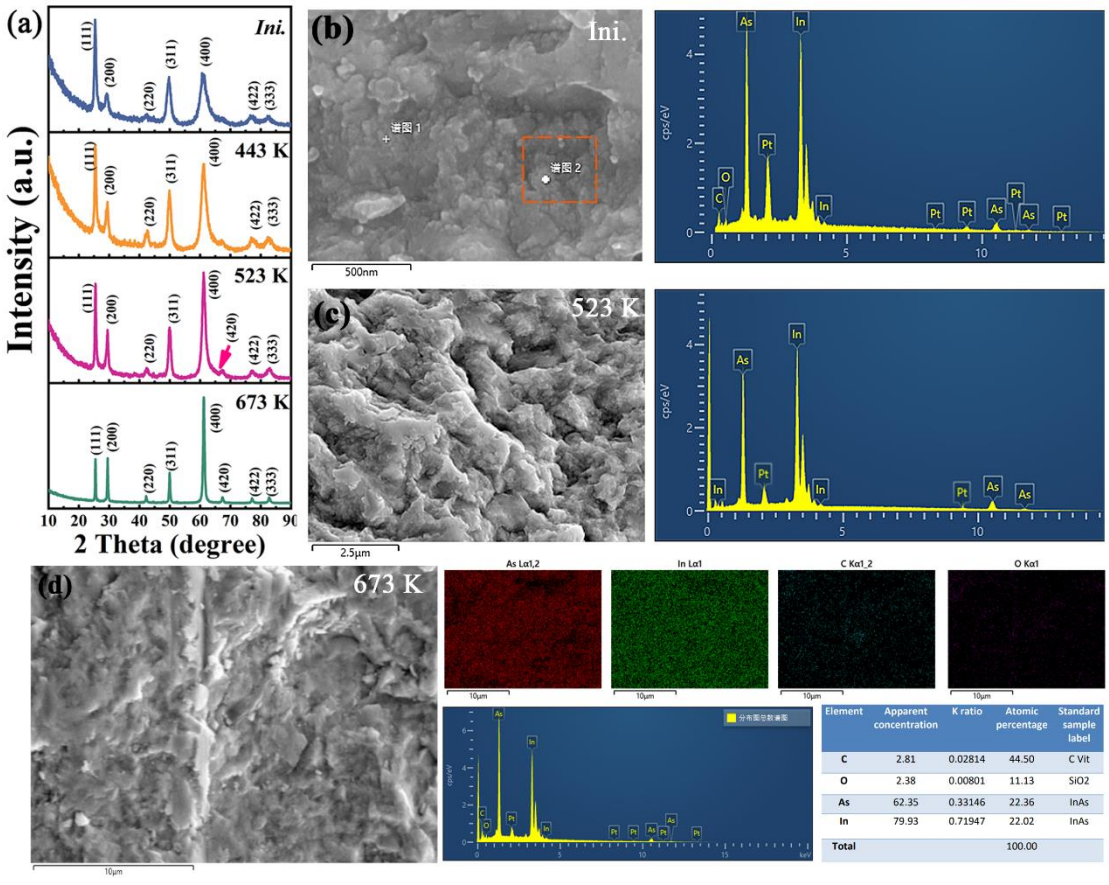

Fig.S3 (a) XRD patterns of the annealed sample under different treatment temperature, (b-d) fresh fracture surface for annealed sample together with spot sweep and area scan maps for EDS. The inserted Table shows the surface chemical composition of SEM image in Fig.S2(d).

Fig.S3(a) shows the XRD patterns of the annealed sample under different treatment temperature, and the details information including FWHM and peak positions of each plot have been extracted in Fig.3(a) and Fig.3(e). It can be seen that the samples are pure InAs-I phase under all processing conditions, and no contaminating phase can be observed. Fig.S3 (b-d) shows the SEM and corresponding EDS scan images of the initial, 523 K, and 673 K processed samples. The scan results showed that all the scanned surfaces were chemically pure (except for Pt conductive coating and atmospheric adsorption elements). The results of the area scan in Fig.S3(d) showed the uniformity of the distribution of As and In elements, while their atomic ratio was about 1 (22.36% / 22.02%). The above results show the phase purity, phase distribution and pore distribution of the sample, which is quite important to confirm the reliability of the hardness test results.